



## Short communication

## Carbon deposition on nickel cermet anodes of solid oxide fuel cells operating on carbon monoxide fuel

Chen Li, Yixiang Shi, Ningsheng Cai\*

Key Laboratory for Thermal Science and Power Engineering of Ministry of Education, Department of Thermal Engineering, Tsinghua University, Beijing 100084, China

## HIGHLIGHTS

- Carbon deposition degree variation with discharging time, temperature and CO mole fraction.
- Distinguished differences between the CO and CH<sub>4</sub> deposited carbon characteristics.
- Carbon mainly deposited on the Ni surface for CO with mainly regular crystal graphitic carbon structure.

## ARTICLE INFO

## Article history:

Received 23 July 2012

Received in revised form

8 October 2012

Accepted 9 October 2012

Available online 16 October 2012

## Keywords:

Carbon deposition

Electrochemical reaction

Solid oxide fuel cell

Anode

Carbon monoxide

## ABSTRACT

Carbon deposition characteristics of CO/CO<sub>2</sub> fuel on an anode support button cell are investigated. The anodic carbon deposition degree increases with the discharging time, the operation temperature and the CO mole fraction in anode gas. The deposited carbon on the anode cross-sections is characterized by an X-ray photoelectron spectroscopy and a Raman spectrometer to analyze the differences and similarities of CO and CH<sub>4</sub> deposited carbon microstructure. The carbon is mainly deposited on the Ni surface for CO while the deposited carbon consists of carbon on the Ni surface and carbonyl group C=O for CH<sub>4</sub>. Not similar to CH<sub>4</sub>, there is no obvious disordered carbon peak in the CO deposited carbon Raman spectra. The CO deposited carbon is mainly in regular crystal graphitic carbon structure and rarely in amorphous carbon structure.

© 2012 Elsevier B.V. All rights reserved.

## 1. Introduction

Solid oxide fuel cells (SOFCs) are well known for their fuel flexibility and tolerance to carbon monoxide, besides their high efficiency, low environmental impacts and system simplicity for stationary or mobile applications [1]. Nickel based cermet anode (e.g. Nickel/yttrium-stabilized zirconia (Ni/YSZ) anode, Ni/scandium-stabilized zirconium (ScSZ) anode) is the most commonly used SOFC anode material ascribe to the advantages of Ni in high electronic conductivity, high catalytic activity and good thermal stability at high temperature [2–4]. However, the Ni metal is also a catalyst of carbon deposition reactions in SOFC anode when fueled with CH<sub>4</sub> or CO [5,6]. The carbon deposition reactions include: the methane cracking reaction as shown in Eq. (1), the reverse Boudouard reaction as shown in Eq. (2), and the reduction of carbon monoxide as shown in Eq. (3), respectively [7–9].



The deposited carbon will occupy the Ni surface reaction active sites, and then deteriorate the catalytic activity of Ni cermet electrode [10]. And the anode pore structure can be damaged by deposited carbon [11], which further accelerates the SOFC anode performance degradation.

Extensive researches have been focused on the SOFC anode carbon deposition process and carbon deposition inhibition strategy for CH<sub>4</sub> and other types of hydrocarbon fuels. Existed researches in published literature are mainly focused on the kinetics of hydrocarbons internal reforming [12–14], the impact of carbon deposition on the anode microstructure [15] and the effects of carbon deposition on cell performance [16], inhibition of carbon deposition by optimizing the operating condition and by adding different elements (CeO<sub>2</sub>, CuO) in SOFC anode [16,17], etc.

\* Corresponding author. Tel./fax: +86 10 62789955.

E-mail addresses: cains@mail.tsinghua.edu.cn, cains@tsinghua.edu.cn (N. Cai).

However, it should be noted that compared with the studies in CH<sub>4</sub> carbon deposition characteristics on Ni/YSZ anode, relative few studies have been focused on the CO carbon deposition characteristics on Ni/YSZ anode. Due to the difference of reaction routes between CH<sub>4</sub> and CO carbon depositions, the deposited carbon morphology and inhibition strategies are quite different [18–21]. Therefore, it is important to clarify the characteristics of CO carbon deposition on the Ni surface and to experimentally test the effects of operating conditions on CO carbon deposition degree on the Ni surface.

In this paper, the carbon deposition behavior of CO/CO<sub>2</sub> fuel on an Ni/YSZ porous anode support button cell has been experimentally investigated with various discharging time, operation temperature and fuel component (CO/CO<sub>2</sub>). Then, the deposited carbon on the anode cross-sections was characterized by an X-ray photoelectron spectroscopy (XPS) and a Raman spectrometer. The XPS and Raman spectra were deconvoluted using pure Gaussian peaks with the same maximum bandwidths. Finally, the comparative analysis of the CH<sub>4</sub> and CO deposited carbon morphology and microstructure have been obtained.

## 2. Experiments

### 2.1. Anode-supported button cell

An anode-supported SOFC button cell made by SICCAS (Shanghai Institute of Ceramics, Chinese Academy of Sciences) was employed. It consists of a Ni/YSZ anode support layer (680 μm), a Ni/scandium-stabilized zirconium (ScSZ) anode active interlayer (15 μm), a ScSZ electrolyte layer (20 μm), and a lanthanum strontium manganate (LSM)/ScSZ cathode layer (15 μm) [22]. The cathode layer is 1.4 cm in diameter and all other layers are 2.6 cm in diameters. The anode support layer and active layer were prepared by mixing nickel oxide (NiO) powder (Inco Ltd., Canada) with 8 mol% YSZ powder (Tosoh, Japan) and with ScSZ powder (Zr<sub>0.89</sub>Sc<sub>0.1</sub>Ce<sub>0.01</sub>O<sub>2-x</sub>, Daiichi Kigenso Kagaku Kogyo, Japan) respectively. The powders were mixed at 50 wt% NiO and 50 wt% stabilized zirconia (YSZ or ScSZ). The electrolyte substrate was a dense film of ScSZ powder. All the ceramic powders were homogenized in a planetary mill with methyl ethyl ketone and ethanol (dispersant) to slurries. Besides, rice starch, polyvinyl butyral, polyethylene glycol and dibutyl o-phthalate were added into the anode layers slurries, which were used as pore former, binder and plasticizer. After being vacuumed for 2 min, the ScSZ, NiO–ScSZ and NiO–YSZ slurries which were used to form electrolyte, anode active and support layers, were cast onto the glass plate by tape casting in sequence. After drying overnight at room temperature, the multilayer tape was detached and co-sintered at 1400 °C in air for 4 h. Then the button cells were cut out from the whole sintered plate. Therefore, the anode and electrolyte layers of all cells were fabricated in one time, which compensates the performance differences caused by cell to cell variations in fabrication to a certain extent. The cathode material was similarly made into paste by mixing LSM (Inframet Advanced Materials, USA) and ScSZ powders in a mass ratio of 50:50. Then, the paste was screen-printed onto the ScSZ layer of button cell and sintered at 1200 °C for 3 h to form the cathode. The button cells were cut directly from one large cell plate so the anode and electrolyte layers of all cells were fabricated at the same time; thus eliminating the anodic material differences caused by cell to cell variations in experimental tests. Before testing, silver paste was reticulated on the anode and cathode surface by screen-printing for current collection. A test setup was constructed to provide the experimental condition for the button cell operation on carbon monoxide fuel [22].

### 2.2. Experimental conditions and procedures

The experiments focused on the impacts of temperature, discharging time and anode gas compositions on the anodic carbon depositions. A mixture of CO/CO<sub>2</sub> was used as the fuel of SOFC button cell and the cell was kept discharging at 0.7 V. The detailed descriptions of the experimental conditions are shown in Table 1.

Before carbon deposition experiments, pure H<sub>2</sub> was fed into the chamber for 1 h to fully reduce the Ni anode and later Ar was used as purging gas for 1 h. During the actual testing, the flowrates of both fuel and oxidant (pure O<sub>2</sub>) were kept at 100 ml min<sup>-1</sup>. Finally, the cell was cooled down to ambient using Ar (150 ml min<sup>-1</sup>) and H<sub>2</sub> (3 ml min<sup>-1</sup>) as protecting gas. Here, about 2% H<sub>2</sub> was added to maintain a reducing atmosphere in the anode chamber to prevent oxidization of the carbon deposited in the anode. Following three cases were used as control experiments for the comparisons between carbon deposition characteristics of CH<sub>4</sub> and CO. (Table 2).

After the tests, the surface morphology and elemental distribution in the anode cross-sections were characterized using a scanning electronic microscope (SEM) and an energy dispersive spectrometer (EDS) with an electron probe microanalyzer (JSM-6460, JEOL, Tokyo, Japan). The surfaces of the anode cross-sections were analyzed by an X-ray photoelectron spectroscopy (XPS) (PHI Quantera, ULVAC-PHI, Kanagawa, Japan) with a monochromatic Al K $\alpha$  ( $h\nu = 1486.7$  eV) X-ray source. To avoid any influence of carbon contamination during the sample transfer and handing, all the sample surfaces were peeled 1.2 nm by an electron gun before characterization. The spot size for analysis was 300 μm × 300 μm. To compensate for the surface-charge effects, the binding energy scale was calibrated with reference to the binding energy of O1s at 530.2 eV. The survey scans were acquired between 1200 and 0 eV. Concurrent region sweeps for O1s, Ni2p, Zr3d, Y3d, and C1s were also obtained. The elemental surface composition was calculated using the transmission values with relative sensitivity factors specific for the instrument equipped with an Al source. The deposited carbon on the anode cross-sections was measured by a Raman Spectrometer (RM2000, Renishaw, New Mills, UK). The excitation line was provided by an Ar<sup>+</sup> laser at 515 nm. The Raman spectra were acquired in the range of 1000–1800 cm<sup>-1</sup>.

## 3. Results and discussion

### 3.1. Characterization of anode carbon deposition

Fig. 1 shows the SEM micrographs of the anode cross-sections for CH<sub>4</sub> 800 °C and CO 8 h cases. The SEM micrographs and surface element distribution maps of the anode cross-sections for the CH<sub>4</sub> carbon deposition have been reported in detail in the previous paper [23]. It is difficult to investigate the morphological nature of the CO and CH<sub>4</sub> deposited carbon on the anode surface in

**Table 1**  
Experimental conditions for the anode carbon deposition.

Cases	Temperature (°C)	Discharging time (h)	Anode gas compositions (%)	
			CO	CO <sub>2</sub>
CO 0.5 h	750	0.5	90	10
CO 2.0 h	750	2.0	90	10
CO 8.0 h	750	8.0	90	10
CO 90%	750	8.0	90	10
CO 50%	750	8.0	50	50
CO 10%	750	8.0	10	90
CO 750 °C	750	8.0	90	10
CO 800 °C	800	2.0	90	10
CO 850 °C	850	2.0	90	10

**Table 2**

Control experiments for the anode carbon deposition.

Cases	Experimental procedures
CH <sub>4</sub> 800 °C	The button cell was discharged at 0.7 V for 30 min using 100 ml min <sup>-1</sup> CH <sub>4</sub> as the anode gas after being reduced by H <sub>2</sub> and purged by Ar. Then, the button cell circuit was opened and the anode gas flowrate was changed to 150 ml min <sup>-1</sup> Ar + 3 ml min <sup>-1</sup> H <sub>2</sub> and purged for 30 min. Finally, the cell temperature was reduced to ambient temperature at 1.5 °C min <sup>-1</sup> with the protection of Ar and H <sub>2</sub> .
Control case 1	The button cell circuit was kept open and the anode gas flowrate was set to 150 ml min <sup>-1</sup> Ar + 3 ml min <sup>-1</sup> H <sub>2</sub> after being reduced by H <sub>2</sub> . Then, the temperature was reduced to ambient temperature at 1.5 °C min <sup>-1</sup> with the protection of Ar and H <sub>2</sub> .
Control case 2	The button cell circuit was kept open with 100 ml min <sup>-1</sup> O <sub>2</sub> as the anode gas, which made the anode fully oxidized. Then, the anode gas flowrate was switched to 100 ml min <sup>-1</sup> H <sub>2</sub> to reduce the anode. Finally, the anode gas flowrate was switched to 150 ml min <sup>-1</sup> Ar + 3 ml min <sup>-1</sup> H <sub>2</sub> and the temperature was reduced to ambient temperature at 1.5 °C min <sup>-1</sup> .

**Fig. 1(a)** and **(b)**. Especially, it is difficult to distinguish the different carbon structures on the surface by SEM. One reason is that the SOFC anode is a kind of cermet, and its local electronic conductivity is poor. The figure will be blurred when the scaling factor is larger than 5000 even spaying gold layer on the sample surface, and the microstructure of the deposited carbon cannot be observed as a result. In addition, the amount of the CO deposited carbon was too small to be precisely detected by the EDS compared to that of the

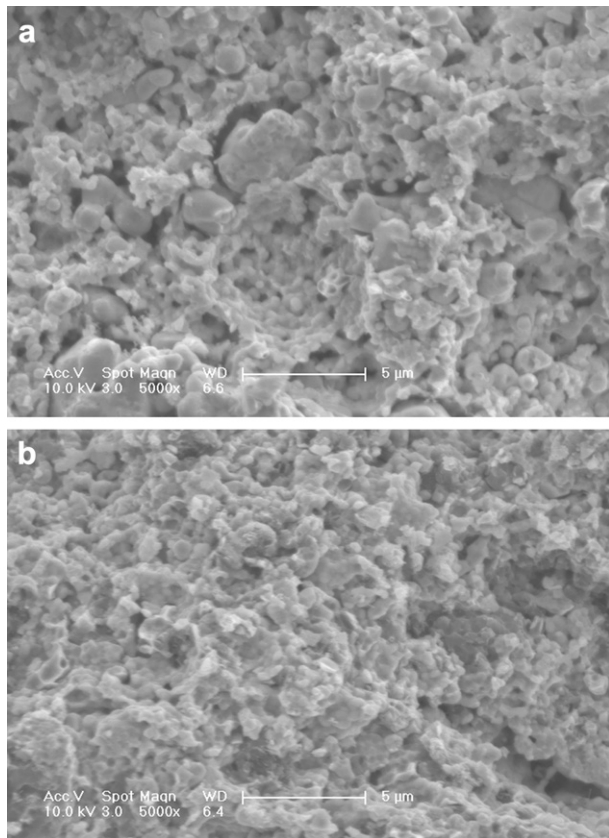


**Fig. 1.** SEM micrographs of the anode cross-sections for (a) CH<sub>4</sub> 800 °C and (b) CO 8 h cases.

CH<sub>4</sub>; thus, the EDS surface element distribution maps of the CO anode carbon deposition similar to the CH<sub>4</sub> carbon deposition in the literature [23] could not be obtained.

Since the error of EDS analysis in detecting the low atomic weight elements (C, O, etc.) is relatively large, and the results are usually quasi-quantitative, whereas the XPS measurements for low atomic weight elements are relatively more accurate. In addition, the large testing spot used in the XPS measurements could well reduce the accidental errors caused by test position. Here, XPS was used to further characterize the anodic carbon deposition with the XPS elemental analysis results for the anode cross-sections. Fig. 2 gives the XPS survey spectra for the anode cross-sections in various discharging time conditions. The atomic percentages in the anode cross-sections for all cases are listed in Table 3.

The XPS elemental analysis results for Control case 1 indicate that there is still a little carbon in the anode after the H<sub>2</sub> reduction even without CO carbon deposition. This is because rice starch was used as pore former in the cell fabrication process and residual carbon was not completely oxidized in the cell sintering process. The carbon percentages for Control cases 1 and 2 show that the anode carbon content was significantly reduced after being oxidized for 8 h in the pure O<sub>2</sub> atmosphere at high temperature, which further proves that the residual carbon without deposition was introduced by the incompletely oxidized pore starch. When the button cell was operated at 750 °C and fueled with 90% CO, the C atomic percentage in the anode increased with the discharging time and was higher than that in Control case I. The Boudouard reaction was not balanced in 8 h. When discharging 2 h with 90% CO, the C atomic percentage and carbon deposition degree in the anode decreased with the increasing of operation temperature. Since the Boudouard reverse reaction is exothermic, from the thermodynamic point of view, the Boudouard reaction occurs more easily at low temperatures and results in more serious carbon deposition. Therefore, high operation temperature cannot only improve the SOFC performance, but also effectively inhibit the anode carbon deposition when fueled with CO, which is exactly the opposite with the SOFC fueled with CH<sub>4</sub>. When discharging 8 h at 750 °C, the C atomic percentage in the anode increased with the increasing of CO mole fraction in anode gas. The ratio of CO and CO<sub>2</sub> concentration increased to promote the Boudouard reaction reverse.

### 3.2. XPS characterization of the anode cross-sections

XPS was used to characterize the near-surface element states in the anode cross-sections after the tests. The XPS surface spectra for O, Ni, Zr, Y and C are shown in Fig. 3. Control case 2 is given as the

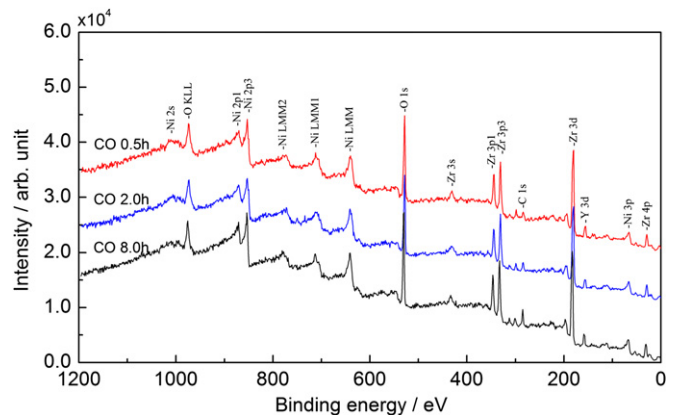


**Fig. 2.** XPS survey spectra for the anode cross-sections in various discharging time conditions.

**Table 3**  
XPS elemental analysis results for the anode cross-sections.

Parameters	Atomic percentage (at %)				
	C	O	Ni	Zr	Y
Discharging time (h)	0.5	10.90	55.93	14.15	16.93
	2.0	12.87	56.56	11.71	16.54
	8.0	14.32	54.18	12.78	16.60
Temperature (°C)	750	12.87	56.56	11.71	16.54
	800	11.60	58.18	11.62	16.38
	850	10.72	57.52	13.30	16.39
CO mole fraction (%)	90	14.32	54.18	12.78	16.60
	50	12.82	58.15	10.28	16.55
	10	10.77	56.29	12.18	18.26
Control case 1		6.38	58.23	15.01	17.92
Control case 2		2.60	60.04	15.71	18.75
CH <sub>4</sub> 800 °C		26.02	48.89	8.87	15.33
					1.89

control data for the XPS spectra for the anode without carbon deposition. The binding energy for O was near 530.2 eV, which corresponds to the O1s orbital of ZrO<sub>2</sub>. The O1s peak of the carbonyl group C=O was not detected in Fig. 3(a) because the carbonyl group C=O content was relatively small near the surface and the corresponding binding energy (530.1 eV) was very close to that of ZrO<sub>2</sub>. The peak for Ni2p<sub>3/2</sub> was observed at a binding energy of 852.4 eV indicating that Ni was in its elemental form after H<sub>2</sub> reduction. The comparisons in Fig. 3(b) show that control case 2 had the largest Ni2p<sub>3/2</sub> peak area because the carbon deposited on the Ni surface was reduced and more Ni surface was exposed. As shown in Fig. 3(c), the XPS spectra for Zr3d contained a doublet at binding energies of 184.6 and 182.2 eV, which can be assigned as the Zr3d<sub>5/2</sub> and Zr3d<sub>3/2</sub> lines. In addition, the Y3d<sub>3/2</sub> peak in Fig. 3(d) is near 157.4 eV, which is in good agreement with the standard peak for the YSZ (Y<sub>2</sub>O<sub>3</sub> + ZrO<sub>2</sub>) anode material. The peak for C1s was observed at a binding energy near 284.7 eV. The

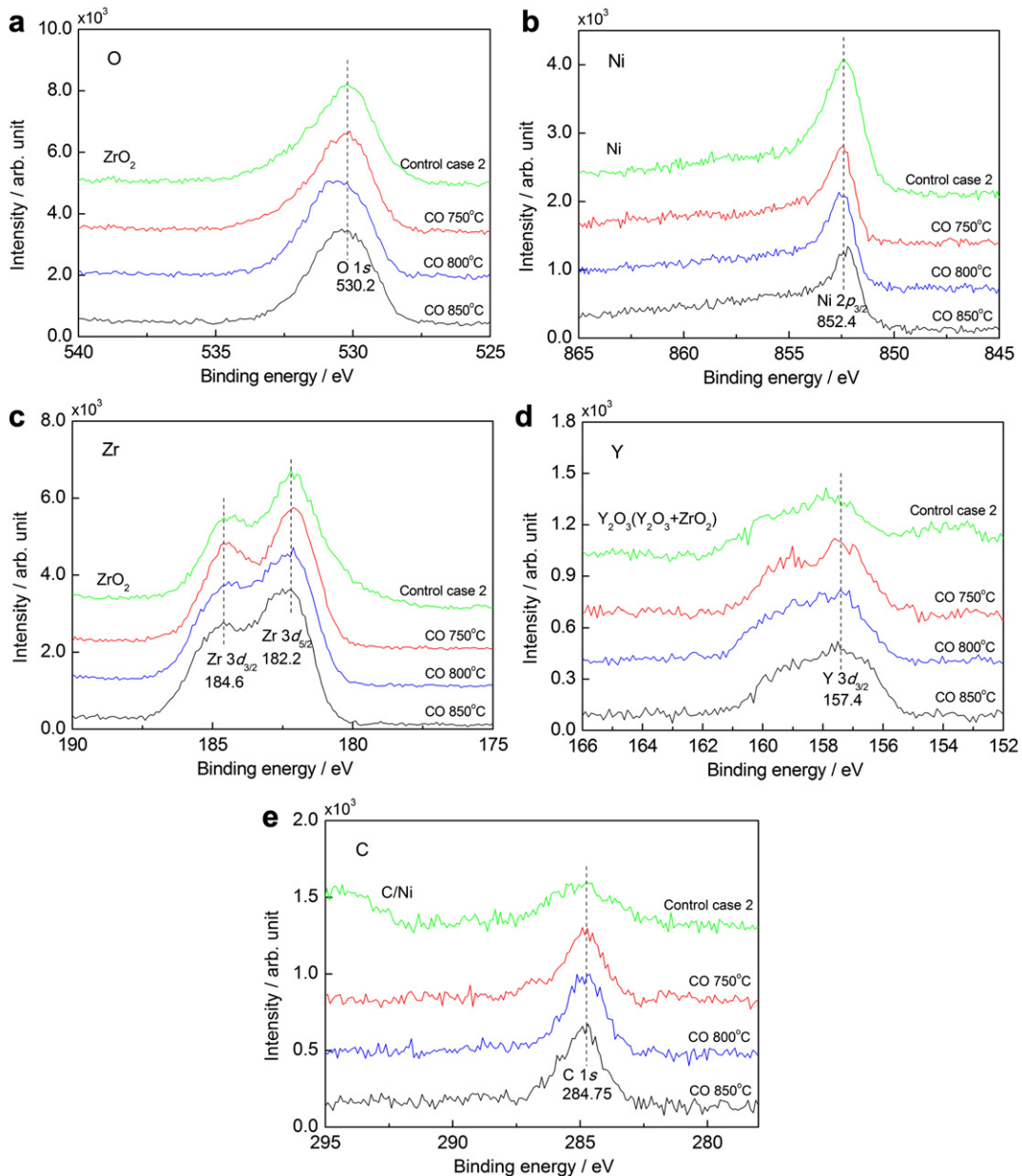


**Fig. 3.** XPS spectra for (a) O1s, (b) Ni2p<sub>3/2</sub>, (c) Zr3d<sub>3/2</sub>, 3d<sub>5/2</sub>, (d) Y3d<sub>3/2</sub> and (e) C1s in various temperature conditions.

comparisons in Fig. 3(e) show that the C1s peak area of CO cases are larger than that of Control case 2, which qualitatively indicates the presence of CO carbon deposition again.

The carbon on the anode cross-section was the focus of the XPS characterization. The C1s XPS peak was deconvoluted using pure Gaussian peaks with the same maximum bandwidths for each given case. Fig. 4 shows the deconvolution of the C1s XPS spectra for control case 2, CO 800 °C and CH<sub>4</sub> 800 °C case.

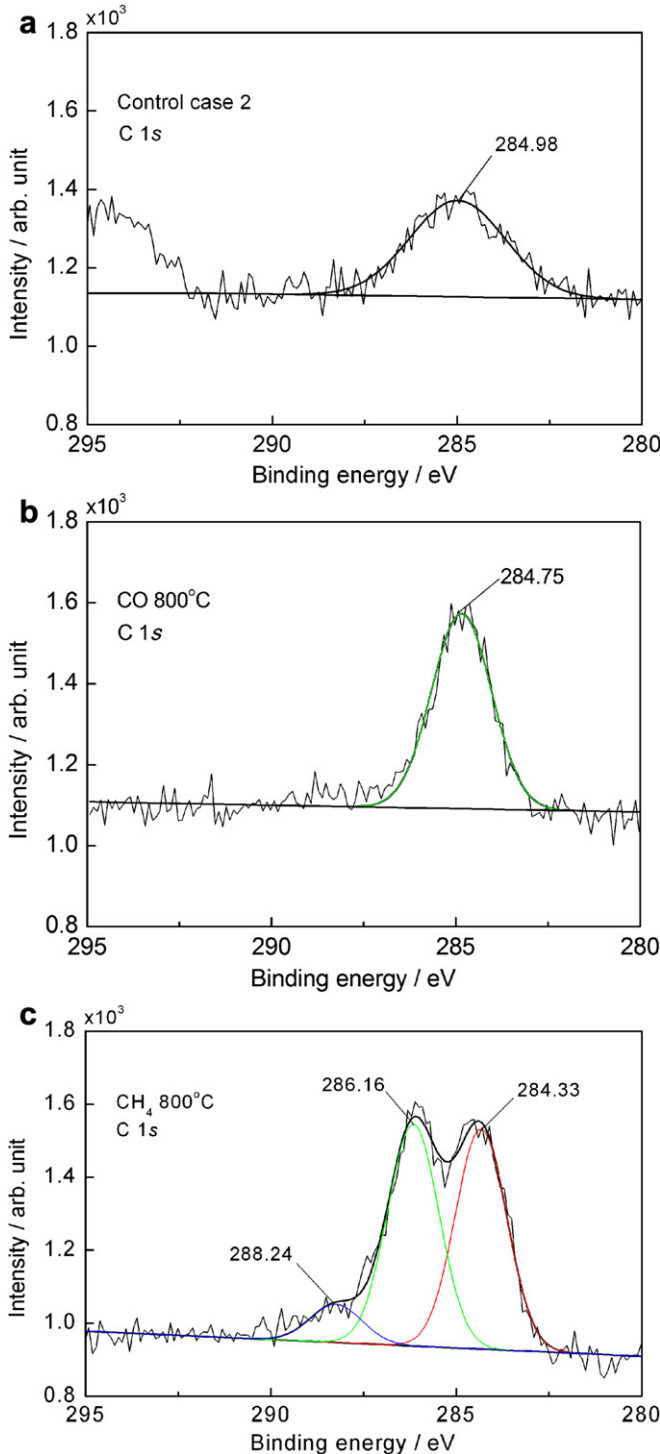


**Fig. 4.** Deconvolution of C1s XPS spectra for various conditions: (a) Control case 2, (b) CO 800 °C and (c) CH<sub>4</sub> 800 °C.

In the standard carbon spectra, the binding energy of C1s for carbon deposited on a Ni surface, C/Ni, is 284.7 eV while the binding energy of C1s in the carbonyl group C=O in most materials is about 286.3 eV. In Control case 2, the peak for C1s was observed at 284.98 eV. The noise ratio in the spectrogram is relatively large due to the low carbon content. Fig. 4(b) shows that only the C/Ni peak was observed with a binding energy of 284.75 eV after the discharging. The results indicate that the carbon is deposited mainly on the Ni surface. In contrast, as shown in Fig. 4(c), after the carbon deposition from CH<sub>4</sub> during the 0.7 V discharging for 30 min, the XPS spectra for C1s showed significant double peaks (at 284.33 and 286.16 eV) corresponding to C/Ni and C=O. The peak at 288.24 eV was within the curve fit accuracy and could be treated as a fitting error. The difference of XPS spectra can be used to distinguish the CO and CH<sub>4</sub> carbon deposition. For the carbon deposition process of CH<sub>4</sub> decomposition, part of the deposited carbon reacted with O<sup>2-</sup> in YSZ and formed carbonyl group C=O. For the CO carbon deposition process, the deposited carbon is formed through Boudouard reaction. The absence of the carbonyl structure C=O indicates that the deposited carbon is difficult to be consumed by direct electrochemical reaction.

The deconvolution results for the C1s XPS spectra for various conditions are listed in Table 4. The half peak width represents the intensity of the carbon excitation. A small half peak width indicates high excitation intensity and large carbon content. The half peak widths in Table 4 show that the carbon contents on the anode cross-sections for various cases decreased in order of CH<sub>4</sub> 800 °C > CO 800 °C > control case 2, which is consistent with the results in Section 3.1.

### 3.3. Raman characterization of deposited carbon in the anode

Raman spectroscopy has been used extensively to characterize the structural features of carbonaceous matters since Tuinstra et al. [24] in 1970 first correlated the Raman bands to structural parameters measured from XRD for polycrystalline graphite. The G (graphite) and D (defect) bands of the Raman spectra are generally used to investigate the carbon structure and to correlate other characteristics. However, Raman spectra cannot give quantitative results for the structural parameters by simply considering the G and D bands, mainly due to the large 'overlap' between these two 'bands'. Structural defects may originate from many structural features in disordered carbon materials. In particular, much structural information can be hidden in the 'overlap' between the G and D bands for highly disordered carbonaceous materials but the G and D bands of highly disordered carbonaceous materials are too broad to have definite meaning. Therefore, deconvolution (curve fits) of the Raman spectra has been used in some studies to acquire more detailed information about the carbon structures [25–27].

Here, the Raman spectra of the deposited carbon on the anode cross-sections were characterized in a range of 1000–1800 cm<sup>-1</sup> and deconvoluted using 6 bands according to the present experimental results and studies in the literature. For highly disordered carbonaceous materials, the G band at 1580–1600 cm<sup>-1</sup> [25] and

**Table 4**  
Deconvolution results of the C 1 s XPS spectra for various conditions.

Cases	C 1 s deconvolution results				
	Formation	Binding energy (eV)	Half peak width (eV)	Area	Percentage (%)
Control case 2	C/Ni (284.7 eV)	284.98	3.04	794.8	100
CH <sub>4</sub> 800 °C	C/Ni (284.7 eV)	284.33	1.63	1047.1	49.8
	C=O ( $\approx$ 286.3 eV)	286.16	1.63	1055.0	50.2
CO 800 °C	C/Ni (284.7 eV)	284.84	1.90	977.7	100

**Table 5**

Raman band assignment summary for the anodic deposited carbon.

Band name	Band position ( $\text{cm}^{-1}$ )	Band type	Description
D	1350	$\text{sp}^2$	Highly disordered carbonaceous materials; C–C bonds between aromatic rings and aromatics with no less than 6 rings
$G_R$	1540	$\text{sp}^2$	Aromatics with 3–5 rings; amorphous carbon structures
$G_1$	1583	$\text{sp}^2$	Graphite; alkene C=C
$G_2$	1600	$\text{sp}^2$	
$G_{L1}$	1680	$\text{sp}^2$	Carbonyl group C=O
$G_{L2}$	1741	$\text{sp}^2$	

the D band at  $1335\text{--}1355 \text{ cm}^{-1}$  [27] are usually referred to as the Graphite and Defect bands. Here, the G band from the deconvolution results showed two peaks, assigned as  $G_1$  and  $G_2$ . Li et al. [25] pointed out a  $G_R$  band at  $1540 \text{ cm}^{-1}$ , which represents aromatic structures with 3–5 rings in amorphous carbon materials. The  $G_L$  band at  $1700 \text{ cm}^{-1}$  represents the carbonyl group C=O [28] with slight differences in the  $G_L$  band for different carbonaceous materials. The  $G_L$  band has been known to have two peaks at  $1680 \text{ cm}^{-1}$  and  $1745 \text{ cm}^{-1}$  [29,30], which is consistent with the present experiment results. These were assigned as  $G_{L1}$  and  $G_{L2}$ . The assignments of the 6 bands are summarized in Table 5.

As indicated in Section 3.1, there was residual carbon in the anode introduced by the incompletely oxidized pore starch. Fig. 5 shows the Raman spectra for anode cross-sections for the control cases. There are no obvious peaks in the Raman spectra besides the measurement noise.

Generally, the residual carbon (due to incomplete oxidized pore starch) does not significantly affect the identification of  $\text{CH}_4$  and CO deposition processes due to two reasons. First, it can be seen from the experimental results of the control cases that the absolute value of residual carbon detection from XPS and Raman spectra is negligible. Second, the cell preparation process in Section 2.1 shows that the residual carbon cannot be oxidized even after  $1400^\circ\text{C}$  calcinations for 4 h and  $1200^\circ\text{C}$  calcinations for 3 h in air atmosphere; thus, the residual carbon should be in the death pore of Ni/YSZ cermet electrode which is hard to contact with oxygen. The residual carbon theoretically cannot appear on the surface of Ni, YSZ or TPB. In this condition, the CO and  $\text{CH}_4$  in gas state have little possibility to interact with the residual carbon.

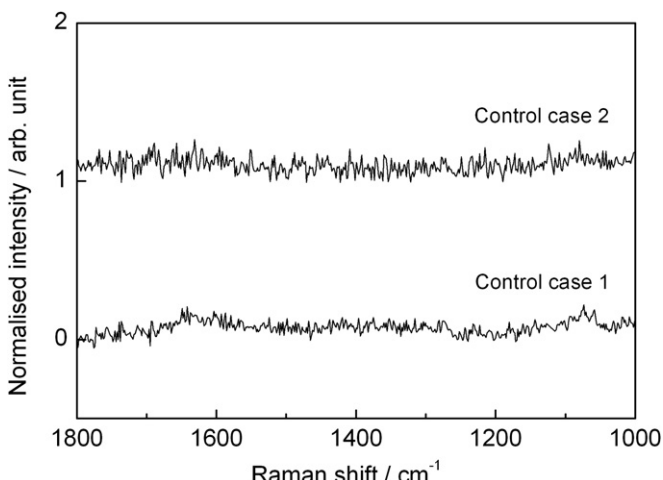


Fig. 5. Raman spectra for the anode cross-sections for the control cases.

It should be noted that although the detection limit of XPS and Raman spectra is very close, in our experimental results for the control cases, the carbon is detected by the XPS while not by Raman, which is mainly due to the difference of the testing procedure, especially due to the pre-treatment process of the samples. According to the above analysis, the residual carbon is holed in the death pore of Ni/YSZ cermet. In the XPS testing process, in order to avoid the contamination to the sample surface during preservation, the sample surface was peeled 1.2 nm by electron gun. After the pre-treatment of the sample, some of the residual carbon in the death pore will be exposed to the atmosphere and can be detected. However, the surface cannot be pre-treated by electron gun in the Raman testing, which is different from the XPS detection; thus, the carbon in the death pores cannot be detected. In fact, this difference in XPS and Raman experimental results further approved the deduction that the residual carbon is holed in the death pore of Ni/YSZ cermet.

The Raman spectra of the deposited carbon in the range of  $1000$  and  $1800 \text{ cm}^{-1}$  were deconvoluted using these bands with 6 pure Gaussian peaks using the Peakfit software. During the curve fitting, the band positions were fixed while the bandwidths were restrained to the same maximum limits. Fig. 6 shows the Raman spectra deconvolution results for the anodic deposited carbon for various conditions.

The ratio ( $I_D/I_G$ ) of the D band to G band intensities (peak areas) in the Raman spectrum deconvolution has been extensively used as an important parameter to study crystalline or graphite-like carbon structures. Some researchers have correlated the  $I_D/I_G$  ratio with the average in-plane length of carbon crystallite structures [24,31–33]. A decrease in the  $I_D/I_G$  ratio is normally expected with increasing graphitization. Other ratios of band intensity have also been used often. Here, three band intensity ratios,  $I_D/I_G$ ,  $I_{GR}/I_G$  and  $I_{GL}/I_G$ , were used to analyze the Raman spectra. The Raman spectra deconvolution data for anodic deposited carbon is listed in Table 6.

Fig. 6(a) (b) and (c) show that there is no obvious disordered carbon peak D band in the CO deposited carbon Raman spectra. There are carbonyl groups C=O peaks  $G_{L1}$  and  $G_{L2}$  band at about  $1680 \text{ cm}^{-1}$  and  $1745 \text{ cm}^{-1}$ , and a small amorphous carbon speak  $G_R$  band at  $1540 \text{ cm}^{-1}$ . The total graphitic carbon peak G band ( $G_1$  and  $G_2$  band) is slightly offset and appears at  $1600 \text{ cm}^{-1}$ . The Raman spectra deconvolution data indicate that the CO deposited carbon is mainly in regular crystal graphitic carbon structure and rarely in amorphous carbon structure. The anode chamber was always maintained in a strong reducing atmosphere for the carbon deposition cases with no O in the anodic gas. Thus, the existence of the carbonyl group C=O indicates that the direct electrochemical reaction occurred between the  $\text{O}^{2-}$  in the YSZ and the deposited carbon in the anode to form a little double-bonded adsorbed carbonyl group C=O. Noting that the carbonyl group C=O peaks  $G_{L1}$  and  $G_{L2}$  band in the Raman spectra is relatively obvious, which seems are inconsistent with the XPS narrow spectrum analysis results of the C element. That is due to the weak Raman spectra of the overall strength of the CO carbon deposition, and the absolute  $G_{L1}$  and  $G_{L2}$  bands area do not represent a true C=O carbonyl content.

Here, the band intensity ratios  $I_{GR}/I_G$  and  $I_{GL}/I_G$  are used to analyze the Raman spectra. With the increasing of the operation temperature, the  $I_{GL}/I_G$  changes are relatively small and no obvious regular. The results indicate that although the carbon deposition degree reduces with the temperature increasing, but temperature has little effect on the proportion of carbonyl and graphitic carbon. The  $I_{GR}/I_G$  decreases with increasing temperature, which indicates that the amorphous carbon content decreased at high temperature. This is mainly due to the high gasification reaction activity of amorphous carbon, the gasification reaction occurs more easily at high temperatures and the amorphous carbon was consumed.

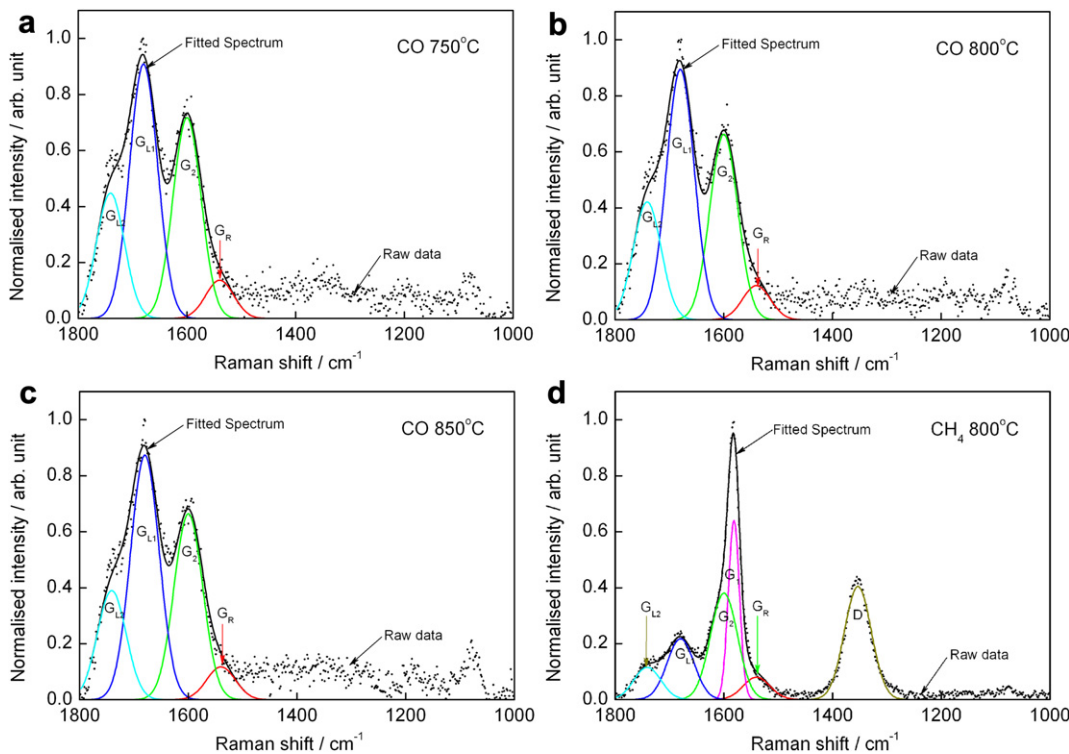


**Fig. 6.** Raman spectra deconvolutions of anodic deposited carbon for various conditions: (a) CO 750 °C, (b) CO 800 °C, (c) CO 850 °C and (d) CH<sub>4</sub> 800 °C.

Fig. 6(d) shows that the deposited carbon structure of CH<sub>4</sub> pyrolysis is quite different from that of CO. There is an obvious disordered carbon peak D band in the CH<sub>4</sub> deposited carbon Raman spectra. Here the total graphitic carbon peak G band consists of obvious G<sub>1</sub> and G<sub>2</sub> band, while the G<sub>1</sub> band in CO deposited carbon Raman spectra is not observed. The parameter  $I_D/I_G$  is the main factor to distinguish the two kinds of deposited carbon. The  $I_G/I_G$  for the CH<sub>4</sub> 800 °C case is smaller than for the CO case, which indicates that the relative content of carbonyl group is smaller in CH<sub>4</sub> deposited carbon.

The difference of the two Raman spectra is caused by the different reaction mechanism of carbon deposition process. It is preliminarily deduced that the main reason is the difference in CO and CH<sub>4</sub> molecule structures resulted from the difference in their C–H bond and C–O bond. The reaction mechanism of CH<sub>4</sub> carbon deposition on the solid Ni surface is assumed to involve the following steps: (1) the decomposition of hydrocarbons over the surface of the metal catalyst through the dissociation of (CH<sub>2</sub>)<sub>n</sub>; (2) the dissolution and diffusion of carbon atoms into the metal phase; (3) precipitation of carbon atoms and the formation of solid carbon.

**Table 6**  
Raman spectra deconvolution data of anodic deposited carbon.

Band information		Cases			
Band name	Band position (cm <sup>-1</sup> )	CO 750 °C	CO 800 °C	CO 850 °C	CH <sub>4</sub> 800 °C
D	1350	/	/	/	27.65
G <sub>R</sub>	1540	6.19	5.82	5.75	5.49
G <sub>1</sub>	1583	/	/	/	18.07
G <sub>2</sub>	1600	32.45	31.54	32.47	26.01
G <sub>L1</sub>	1680	41.11	42.59	42.71	14.87
G <sub>L2</sub>	1741	20.25	20.05	19.06	7.91
$I_D/I_G$		/	/	/	0.627
$I_{GL}/I_G$		1.891	1.986	1.902	0.517
$I_{GR}/I_G$		0.191	0.184	0.177	0.125

In fact, Ni-based anodes are unstable in presence of hydrocarbons because Ni is a catalyst for the formation of carbon fibers. Because these reactions involve more than the Ni surface, carbon fiber formation can lead to loss of Ni by “metal dusting” a process that occurs when Ni is physically lifted from the sample by its attachment to the growing carbon fiber. Fiber growth can also cause fuel cells by fracture because of the mechanical stresses induced by the growth of the fibers [34]. However, CO deposition do not have the above reaction (1). It means that the CO could have more possibilities to get the relatively simple deposited carbon. In addition, it is believed that the carbon deposition and carbonyl group formation is not only related to Ni catalysis, but also related to electrochemical reactions [23].

#### 4. Conclusions

Carbon deposition characteristics of CO/CO<sub>2</sub> gas fuel on Ni cermet anode support button cell were experimentally investigated in this paper. The impacts of discharging time, operation temperature and fuel component (CO/CO<sub>2</sub>) on the anodic carbon deposition at 0.7 V discharging condition were tested. The deposited carbon on the anode cross-sections was characterized by an XPS and a Raman spectrometer to analyze the deposited carbon microstructure.

The anodic carbon deposition degree increased with the discharging time, the operation temperature and the CO mole fraction in anode gas. The carbon is deposited mainly on the Ni surface for CO while the deposited carbon consists of carbon on the Ni surface and carbonyl group C=O for CH<sub>4</sub>. This characteristic in XPS spectra can be used to distinguish the CO and CH<sub>4</sub> carbon deposition. There is no obvious disordered carbon peak in the CO deposited carbon Raman spectra which are not similar to CH<sub>4</sub>. The CO deposited carbon is mainly in regular crystal graphitic carbon structure and rarely in amorphous carbon structure. The total graphitic carbon peak G band consists of obvious G<sub>1</sub> and G<sub>2</sub> band, while the G<sub>1</sub> band

in CO deposited carbon Raman spectra is not observed. Although the carbon deposition degree reduces with the temperature increasing, but temperature has little effect on the proportion of carbonyl and graphitic carbon.

## Acknowledgments

This work was supported by the National Natural Science Foundation of China (20776078, 51106085) and the Seed Funding of Low Carbon Energy University Alliance. We gratefully acknowledge the insightful discussions and the button cells used in experiments produced by Prof. Shaorong Wang of the Shanghai Institute of Ceramics Chinese Academy of Sciences (SICCAS), China.

## References

- [1] Y. Shi, C. Li, N. Cai, *J. Power Sources* 196 (2011) 5526–5537.
- [2] US DOE, Fuel Cell Handbook, seventh ed., DOE/NETL, Morgantown, WV, 2004.
- [3] C. Su, Y. Wu, W. Wang, Y. Zheng, R. Ran, Z. Shao, *J. Power Sources* 195 (2010) 1333–1343.
- [4] D. Storjohann, J. Daggett, N.P. Sullivan, H. Zhu, R.J. Kee, S. Menzer, D. Beeaff, *J. Power Sources* 193 (2009) 706–712.
- [5] M.L. Toebes, J.H. Bitter, A.J. van Dillen, K.P. de Jong, *Catal. Today* 76 (2002) 33–42.
- [6] T. Takeguchi, Y. Kani, T. Yano, R. Kikuchi, K. Eguchi, K. Tsujimoto, Y. Uchida, A. Ueno, K. Omoshiki, M. Aizawa, *J. Power Sources* 112 (2002) 588–595.
- [7] K. Nikooyeh, R. Clemmer, V. Alzate-Restrepo, J.M. Hill, *Appl. Catal. A Gen.* 347 (2008) 106–111.
- [8] C.H. Bartholomew, *Catal. Rev. Sci. Eng.* 24 (1982) 67–112.
- [9] D. Singh, E. Hernandez-Pacheco, P.N. Hutton, N. Patel, M.D. Mann, *J. Power Sources* 142 (2005) 194–199.
- [10] C.M. Finnerty, N.J. Coe, R.H. Cunningham, R.M. Ormerod, *Catal. Today* 46 (1998) 137–145.
- [11] H. He, J.M. Hill, *Appl. Catal. A Gen.* 317 (2007) 284–292.
- [12] M. Cimenti, J.M. Hill, *J. Power Sources* 186 (2009) 377–384.
- [13] Y. Yang, X. Du, L. Yang, Y. Huang, H. Xian, *Appl. Therm. Eng.* 29 (2009) 1106–1113.
- [14] N. Laosiripojana, S. Assabumrungrat, *Appl. Catal. B Environ.* 82 (2008) 103–113.
- [15] C.M. Finnerty, R.M. Ormerod, *J. Power Sources* 86 (2000) 390–394.
- [16] S. McIntosh, J.M. Vohs, R.J. Gorte, *J. Electrochem. Soc.* 150 (2003) A470–A476.
- [17] N. Nakagawa, H. Sagara, K. Kato, *J. Power Sources* 92 (2001) 88–94.
- [18] S. Park, J.M. Vohs, R.J. Gorte, *Nature* 404 (2000) 265–267.
- [19] S. Park, R. Cracium, J.M. Vohs, *J. Electrochem. Soc.* 146 (1999) 3603–3605.
- [20] C. Lu, W.L. Worrell, R.J. Gorte, J.M. Vohs, *J. Electrochem. Soc.* 150 (2003) A354–A358.
- [21] B.C.H. Steele, P.H. Middleton, R.A. Rudkin, *Solid State Ion.* 40/41 (1990) 388–393.
- [22] C. Li, Y. Shi, N. Cai, *J. Power Sources* 195 (2010) 2266–2282.
- [23] C. Li, Y. Shi, N. Cai, *J. Power Sources* 196 (2011) 754–763.
- [24] F. Tuinstra, J.L. Koenig, *J. Chem. Phys.* 53 (1970) 1126–1130.
- [25] X. Li, J. Hayashi, C. Li, *Fuel* 85 (2006) 1700–1707.
- [26] X. Zhu, C. Sheng, *Fuel Process. Technol.* 91 (2010) 837–842.
- [27] N. Larouche, B.L. Stansfield, *Carbon* 48 (2010) 620–629.
- [28] D. Lin-Vien, N.B. Colthup, W.G. Fateley, J.G. Grasselli, *The Handbook of Infrared and Raman Characteristic Frequencies of Organic Molecules*, Academic Press, San Diego, 1991.
- [29] B. Schrader, *Raman/Infrared Atlas of Organic Compounds*, VCH, Weinheim, Germany, 1989.
- [30] R. Singh, *Electrochemical and partial oxidation of CH<sub>4</sub>*, PhD thesis, University of Akron, USA, 2008.
- [31] G.A. Zickler, B. Smarsly, N. Gierlinger, H. Peterlik, O. Paris, *Carbon* 44 (2006) 3239–3246.
- [32] T. Jawhari, A. Roid, J. Casado, *Carbon* 33 (1995) 1561–1565.
- [33] L.G. Cançado, K. Takai, T. Enoki, M. Endo, Y.A. Kim, H. Mizusaki, A. Jorio, L.N. Coelho, R. Magalhães-Paniago, M.A. Pimenta, *Appl. Phys. Lett.* 88 (2006) 163106.
- [34] T. Kim, G. Liu, M. Boaro, S.-I. Lee, J.M. Vohs, R.J. Gorte, O.H. Al-Madhi, B.O. Dabbousi, *J. Power Sources* 155 (2006) 231–238.